J. Fluid Mech. (1972), *vol.* 51, *part* 1, *pp.* 187–205
Printed in Great Britain

Gas and solids motion around deformed and interacting bubbles in fluidized beds

By R. CLIFT, J. R. GRACE,
L. CHEUNG AND T. H. DO

Department of Chemical Engineering,
McGill University, Montreal, Canada

(Received 18 August 1970 and in revised form 26 February 1971)

Previous analyses of gas and particle motion around bubbles in fluidized beds have concentrated on idealized isolated bubbles. In this paper three non-idealities are considered using the theoretical models of Davidson and Murray. Gas flow patterns are derived for indented and elongated bubbles and for pairs of interacting bubbles. Cloud boundaries are predicted for these situations and some effects on gas–solid contacting are discussed.

1. Introduction

Fluidized beds in which the ratio of solids density to the density of the fluidizing fluid is large are characterized by rising fluid pockets or 'bubbles' analogous in many respects to large gas bubbles in liquids (Davidson & Harrison 1963). These bubbles give rise to most of the properties which have led to wide industrial application of gas-fluidized beds; the details of bubble behaviour are therefore of considerable theoretical and practical interest. Several models have been proposed to describe the motion of gas and particles around rising bubbles in fluidized beds (Davidson 1961; Jackson 1963*b*; Murray 1965*b*) but the applications of these models have concentrated on idealized bubbles with spherical or circular boundaries. Real bubbles in fluidized beds seldom, if ever, have these idealized shapes. This paper presents analyses of the gas and particle motion around bubbles associated with particle wakes, elongated or flattened bubbles and interacting bubble pairs. For analytical simplicity the treatment is restricted to two-dimensional bubbles, in the expectation that the results are at least qualitatively applicable to three-dimensional bubbles.

In the majority of gas-fluidized beds the bubble rise velocity U_B exceeds the interstitial gas velocity u_0; the gas within a bubble circulates to and from a limited region of the surrounding particulate phase, termed the 'cloud' (Rowe, Partridge & Lyall 1964). The size of the cloud gives an indication of the effectiveness of contact between bubble gas and the fluidized particles (Rowe 1964). This paper therefore concentrates upon the manner in which bubble distortion and interaction affect the gas cloud.

The first theoretical treatment of clouds was given by Davidson (1961), who assumed that the gas phase is incompressible, that the motion of the interstitial

gas relative to the particles obeys Darcy's Law, and that the particulate phase may be treated macroscopically as an incompressible inviscid fluid. Both the gas flow in the dense phase and the particle motion can then be described by the equations of potential flow. The interstitial gas flow is obtained by superimposing the solids motion and the gas flow which would be present if the particles were fixed in their instantaneous positions. Thus

$$w_G = w_P + w_{G_0}, \tag{1}$$

where w_G, w_P and w_{G_0} are the complex potentials for gas, particles, and gas in the absence of solids movement respectively.

Jackson (1963*a*) and Murray (1965*a*) derived continuity and momentum equations for fluidized beds based on a continuum approach. Their complete equations differ, but both authors made simplifying assumptions for gas-fluidized systems (Jackson 1963*b*; Murray 1965*b*) which make the resulting equations identical, despite different notations which tends to obscure this fact. Jackson (1963*b*) attempted a numerical solution and presented the first iteration. This approach requires formidable numerical calculations to reach even the first step in the iteration process for an ideal bubble; for this reason Jackson's theory is not treated here. For isolated spherical bubbles Jackson's solution predicts clouds which are very similar to those obtained in closed form by Murray.

Murray (1965*b*) linearized the equations for steady motion in such a way that the resulting motion of both gas and particles is irrotational and incompressible. The complex potential for the gas is then an explicit function of the complex potential for the particles,

$$w_G = u_0 z + w_P - CFa(\alpha u_0 + dw_P/dz), \tag{2}$$

where $\alpha = U_B/u_0$, $F = u_0^2/ga$ is a Froude number and a is the bubble radius. Murray chose the constant C so that the gas pressure is constant over the front of the bubble. In all three models the gas density is taken to be negligible. This assumption leads to the requirement that the gas pressure be constant on the surface of the bubble. In fact Murray's model satisfies the constant pressure condition only in the vicinity of the bubble nose, whereas Davidson's model enables the constant pressure condition to be satisfied at all points on the bubble surface.

Experimental cloud sizes and shapes have been found to agree more closely with the predictions of Murray's model than with those of Davidson's (Rowe, Partridge & Lyall 1964). On the other hand, Davidson's model is qualitatively correct and mathematically simpler than Murray's and, as just noted, it gives a more realistic distribution of gas pressure. Both models are used in this paper to treat indented and elliptical bubbles; for analytical reasons only Murray's model is used for interacting bubbles.

2. Bubbles with particle wakes

Real bubbles in fluidized beds adopt a circular-cap or spherical-cap shape with an indented base (Rowe & Partridge 1962, 1965). Observations of particle transport (Rowe & Partridge 1962; Rowe, Partridge, Cheney, Henwood & Lyall 1965)

and bubble coalescence (Clift & Grace 1970, 1971*b*) show that a bubble and its wake may be represented by a circular or spherical cap empty of particles with a wake of particles completing the circle or sphere and travelling with the bubble. In order to describe particle and fluid motion around a two-dimensional bubble we have adopted a procedure suggested by Stewart (1968). Particles are assumed to flow around the complete circle enclosing the bubble and its wake. For Murray's model the gas flow follows directly from (2). For Davidson's model the description of the gas flow is completed by inserting the condition that the gas pressure is constant on the surface of an indented kidney-shaped bubble obtained by conformal transformation of the equations for a circular bubble.† The approach gives a constant gas pressure boundary and a closed solids streamline which are different; this difference distinguishes our treatment from the analysis of a deformed bubble given by Collins (1965). However the pressure field for our indented bubble is identical to that associated with the analysis of Collins since w_{G_0} is common to the two approaches. Stewart (1968) has shown that this pressure field is in excellent agreement, even in the wake region, with measurements obtained by Reuter (1963).

If the vorticity of solids is largely confined to the wake region and if the voidage is substantially constant throughout the dense phase, then the particle motion outside the bubble and its wake may be described by the equations of potential flow.‡ With co-ordinates fixed on the bubble, the boundary conditions are as follows: (i) uniform velocity $-U_B$ at infinity; (ii) no flow across the circular boundary containing the bubble and its wake. If the centre of curvature of the bubble is at x_0 on the real (vertical) axis of the complex plane $z = x+iy$, the complex potential is given by

$$w_P = -u_0\alpha\{(z-x_0)+a^2/(z-x_0)\}. \tag{3}$$

To obtain the complex potential for the gas motion according to Davidson's model it is first necessary to describe the fluid motion for a stationary void. The boundary conditions are as follows: (i) constant interstitial velocity u_0 at infinity, (ii) constant pressure (and hence constant velocity potential ϕ_{G_0}) at the kidney-shaped bubble boundary. Collins (1965) showed that the solution could be obtained using a particular form of the Joukowski transformation

$$z = t-k^2/t. \tag{4}$$

Under this transformation, the circle of unit radius centred at d on the real axis of the t plane,

$$t = d+e^{i\beta}, \tag{5}$$

is mapped into a kidney-shaped bubble in the z plane. The transformed bubble

† This simple approach may be contrasted with Murray's (1965*b*) analysis of a bubble with a steady cusped free-streamline wake. The complexity of Murray's analysis renders it more cumbersome, and the physical model is no more realistic.

‡ The assumption that vorticity is confined within the circular boundary containing the bubble and its wake is consistent with Parlange's (1969) analysis of spherical-cap bubbles in liquids with closed laminar wakes. Voidage increases adjacent to rising bubbles have been found by Lockett & Harrison (1967) but these increases are very small and are therefore ignored in the present treatment.

boundary is a good approximation to the shape of a real kidney-shaped bubble if $k+d=1$. The complex potential which satisfies the above boundary conditions is

$$w_{G_0} = \tfrac{1}{2}u_0[(z-2d+(z^2+4k^2)^{\frac{1}{2}}) - 4/\{z-2d+(z^2+4k^2)^{\frac{1}{2}}\}]. \tag{6}$$

The complex potential for gas motion around the moving bubble now follows from (1). The imaginary part of w_G gives the gas stream function

$$\psi_G = u_0\left[\frac{Y}{2}\left\{1+\frac{4}{X^2+Y^2}\right\} - \alpha y\left\{1-\frac{a^2}{(x-x_0)^2+y^2}\right\}\right], \tag{7}$$

where $X = x+q\cos\delta-2d$, $Y = y+q\sin\delta$, $q^4 = (x^2-y^2+4k^2)^2+4x^2y^2$

and $$\tan 2\delta = 2xy/(x^2-y^2+4k^2).$$

For each value of k, a and x_0 are the radius of curvature and centre of curvature, respectively, of the upper part of the transformed bubble. Table 1 shows the values of a and x_0 for three values of k, determined in each case by fitting the

Transformation constant (k)	0·286	0·35	0·40
Radius of curvature (a)	1·0561	1·0917	1·1287
Centre of curvature (x_0)	0·6106	0·4841	0·3713
Bubble area (A_b)	3·05	3·007	2·955
Shape characteristic ($a/A_b^{\frac{1}{2}}$)	0·605	0·63	0·656
Included angle (approx.)	278°	267°	247°

TABLE 1. Characteristics of transformed bubble

circle through the points corresponding to $\beta = 0$ and $\beta = \pm\frac{1}{2}\pi$. The cloud boundary is obtained from (7) as the closed branch of the streamline $\psi_G = 0$, i.e.

$$\frac{Y}{2}\left\{1+\frac{4}{X^2+Y^2}\right\} = \alpha y\left\{1-\frac{a^2}{(x-x_0)^2+y^2}\right\}. \tag{8}$$

Results are presented here for $k = 0{\cdot}35$ and $0{\cdot}40$ as well as for $k = 0{\cdot}286$, the value employed by Collins. The corresponding bubble shapes can be characterized (as shown in table 1) by the values of the included angle of the circular cap and by the ratio $a/A_b^{\frac{1}{2}}$, where A_b is the bubble area, and correspond to different apparent dense-phase viscosities (Grace 1970).

For Murray's model the complex potential for the fluid motion outside the circular boundary containing the bubble and wake follows directly from (2) and (3), i.e.

$$w_G = u_0 z - U_B\left[(z-x_0)+\frac{a^2}{z-x_0}+\frac{CFa^3\alpha}{(z-x_0)^2}\right]. \tag{9}$$

Equations (2) and (3) are independent of the processes occurring inside the boundary so (9) applies whether a wake is contained within the circular boundary or not. Application of the constant pressure condition in the vicinity of the bubble nose yields (Murray 1965*b*)

$$CF = 1/4\alpha^2. \tag{10}$$

Substituting this relationship into (9) we obtain

$$w_G = u_0\left[z-\frac{a^3}{4(z-x_0)^2}\right] - U_B\left[(z-x_0)+\frac{a^2}{z-x_0}\right]. \tag{11}$$

When (11) is rewritten in polar co-ordinates with origin at the centre of curvature of the bubble the imaginary part of the resulting equation gives

$$\psi_G = \left[(u_0 - U_B)r + \frac{a^2 U_B}{r}\right]\sin\theta + \frac{u_0 a^3}{4r^2}\sin 2\theta. \tag{12}$$

The cloud boundary can now be obtained from (12) as the closed branch of the streamline $\psi_G = 0$, given by

$$\cos\theta + (2r/a)\,[(1-\alpha)r^2/a^2 + \alpha] = 0. \tag{13}$$

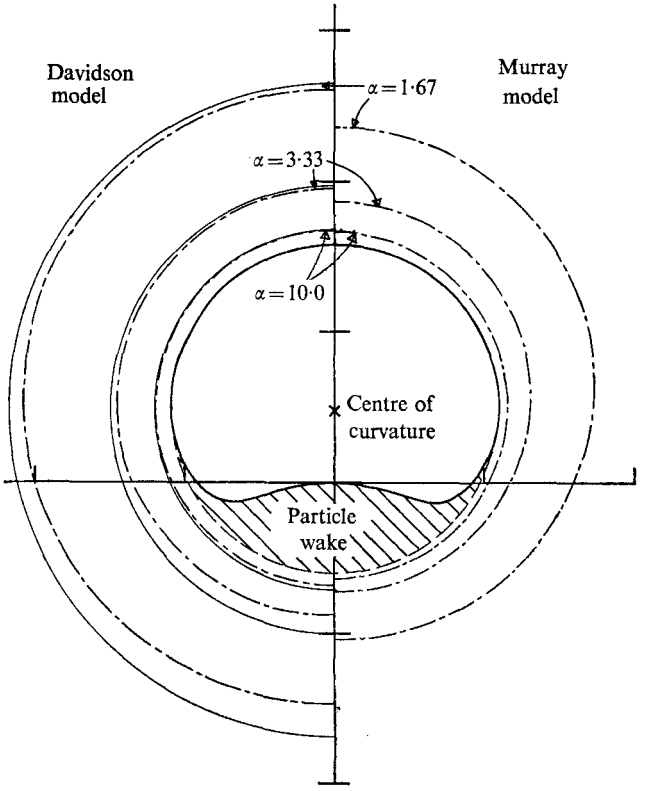

FIGURE 1. Cloud boundaries for indented two-dimensional bubbles as predicted using the Davidson and Murray theories. — · — ·, bubble with wake; —, circular bubble.

Figure 1 shows cloud boundaries for the bubble shape corresponding to $k = 0{\cdot}35$ and three values of α calculated for the Davidson and Murray models from (8) and (13). For the Davidson model the cloud boundaries for the circular bubble with the same radius a and dimensionless velocity α are plotted for comparison. It is clear that the indentation at the rear of a bubble has very little effect on the leading boundary of the cloud, but our analysis shows that the boundary of the cloud is displaced upwards at the rear. As a result, the centroid of the cloud is pushed forward slightly; this is in agreement both with the cloud for the Murray model and with experiment. As noted above, application of the Murray model to the deformed bubble results in a cloud boundary which is identical to the cloud boundary predicted for an undeformed bubble.

Figure 2 shows values of A_c/A_{c_0} plotted as a function of α for the two models and three bubble shapes, where A_c is the cloud area for an indented bubble, the wake being included within the cloud, and A_{c_0} is the cloud area for the circular bubble with the same area and the same value of α. The ratio diverges significantly from unity, especially for large α when the cloud region is relatively thin so that the wake region is the major contribution to A_c. Both models predict that

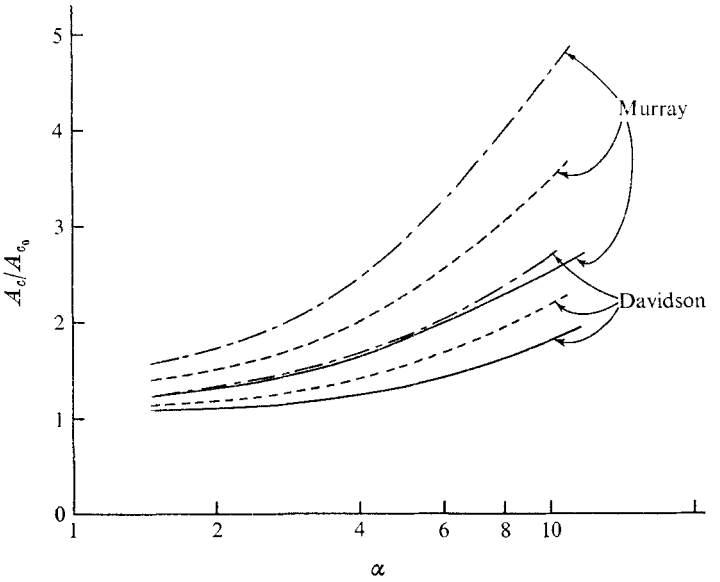

FIGURE 2. Ratio of cloud area for indented bubbles to cloud area for undeformed bubbles as a function of α. —, $k = 0{\cdot}286$; - - - -, $k = 0{\cdot}35$; — · — ·, $k = 0{\cdot}40$.

cloud areas calculated on the assumption that a bubble is circular and wakeless can be greatly in error, especially in the small particle high α systems which are of the greatest practical importance. In chemical reactor modelling, some authors (e.g. Rowe 1964; Kunii & Levenspiel 1969; Pyle & Rose 1965) have allowed for the wake by assuming the cloud boundary to be identical to that predicted for perfectly spherical bubbles, and by adding a wake fraction to be included within the bubble. Our analysis shows that this approximation is justified for the Murray model but that it is not strictly correct for the Davidson approach.

3. Elliptical bubbles

Bubbles undergo frequent deformations in freely bubbling fluidized beds, especially during the process of splitting and coalescence. While an elliptical shape does not model the contour of elongated or flattened bubbles perfectly, this shape allows us to predict qualitatively the effect of deformation on cloud boundaries. Elliptical cylinders with their major axes aligned vertically approximate the shape of bubbles enclosing vertical rods or tubes (Grace & Harrison

1968). It was shown in the previous section that the presence of a wake influences the cloud boundary to a limited extent only; the bubbles in this section are therefore assumed to be perfectly elliptical with no wake indentations.

The bubble is assumed to be elliptical with vertical semi-axis a and horizontal semi-axis b. The focal distance is c, where

$$c^2 = a^2 - b^2. \tag{14}$$

The bubble eccentricity is $e = c/a$ and the ratio b/a is denoted by τ. Thus

$$e^2 = 1 - \tau^2. \tag{15}$$

Defining the complex variable $\zeta = \xi + i\eta$,

where ξ and η are elliptical co-ordinates, and using the transformation

$$z = c\cosh\zeta = c(\cosh\xi\cos\eta + i\sinh\xi\sin\eta)$$

we may write $a = c\cosh\xi_0$, $b = c\sinh\xi_0$, $\tau = \tanh\xi_0$,

where ξ_0 is the constant value of ξ which defines the boundary of the elliptical bubble.

The particle complex potential describing potential flow past this elliptical boundary, with a uniform velocity $-U_B$ at infinity, is given (Milne-Thomson 1962; Grace & Harrison 1967) by

$$w_P = -U_B a(1+\tau)\cosh(\zeta - \xi_0). \tag{16}$$

The imaginary part of (16) gives the particle stream function

$$\psi_P = -U_B a(1+\tau)\sinh(\xi - \xi_0)\sin\eta. \tag{17}$$

For Davidson's model the stream function for the gas motion is obtained from the imaginary part of (1), i.e.

$$\psi_G = \psi_P + \psi_{G_0}, \tag{18}$$

where ψ_{G_0} is the stream function for percolation of gas through a stationary void. This is given (Grace & Harrison 1969) by

$$\psi_{G_0} = u_0 a(1+\tau)\cosh(\xi - \xi_0)\sin\eta. \tag{19}$$

Combining (17), (18) and (19) we obtain

$$\psi_G = (u_0 a(1+\tau)/e)[(1+\alpha\tau)\cosh\xi - (\alpha+\tau)\sinh\xi]\sin\eta. \tag{20}$$

As before, the cloud boundary is the closed branch of the streamline $\psi_G = 0$,

$$\tanh\xi = (1+\alpha\tau)/(\alpha-\tau) \quad (\alpha > 1). \tag{21}$$

Equation (21) defines an elliptical cloud boundary with the same centre and focal length as the bubble. Cloud boundaries for $\tau = 0{\cdot}80$ and $\tau = 0{\cdot}60$ are shown in figure 3. For reference purposes, the clouds for the corresponding circular bubble

of the same area and the same α are also plotted. Clouds for elongated bubbles have a lower eccentricity than the bubbles with which they are associated. More important, they are somewhat larger in area than for the corresponding circular bubbles.† From geometrical considerations it can be shown that the ratio of the major axis of the elliptical cloud a_c to that of the bubble is given by

$$a_c/a = (\alpha+\tau)/(\alpha^2-1)^{\frac{1}{2}}.$$

Similarly the minor axis of the cloud b_c is such that

$$b_c/b = (\alpha+1/\tau)/(\alpha^2-1)^{\frac{1}{2}}.$$

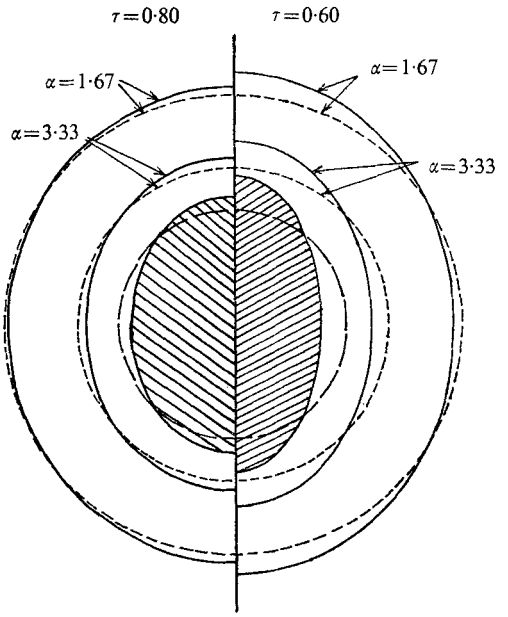

FIGURE 3. Cloud boundaries for elliptical bubbles: Davidson theory. —, cloud boundary for elliptical bubble; ////, elliptical bubble boundary; – – –, boundary of corresponding circular bubble; - - - - -, cloud boundary for circular bubble.

Hence the ratio of the cloud area to the bubble area, an important ratio in determining the effectiveness of gas–solid contact, is given by

$$A_c/A_b = \{2+\alpha(\tau+1/\tau)\}/(\alpha^2-1). \tag{22}$$

Values of A_c/A_b calculated from (22) are presented for four bubble shapes and three values of α in table 2.

The use of (19) in Davidson's model automatically satisfies the condition that the gas pressure be constant at the bubble surface. For Murray's model it is necessary to evaluate CF in order to make the pressure constant at the bubble nose. This in turn requires (Murray 1965*b*) that

$$\mathrm{Re}\{u_0 z - CF\alpha a(\alpha u_0 + dw_P/dz)\} = \text{constant} \quad \text{for} \quad \xi = \xi_0 \quad \text{as} \quad \eta \to 0.$$

† The clouds predicted by Davidson's model for the corresponding flattened bubbles, τ = 1·25 and 1·67, are simply obtained by rotating figure 3 through 90°.

The above condition is satisfied to terms of order η^3 when

$$CF = \left(\frac{\tau^2}{1+\tau}\right) \times \frac{1}{2\alpha^2}. \tag{23}$$

It is helpful to rewrite (16) as

$$w_P = -u_0\alpha\{z + (a^2/c)\tau(1+\tau)(\cosh\xi - \sinh\xi)\}. \tag{16a}$$

Now for Murray's model the complex potential for the gas motion follows from (2), (16*a*) and (23). The imaginary part of the resulting expression gives the gas stream function,

$$\psi_G = u_0 a \sin\eta \left\{(1-\alpha)e\sinh\xi + \frac{\alpha\tau(1+\tau)}{e(\cosh\xi+\sinh\xi)} + \frac{\tau^3}{2e^2} \times \frac{\cos\eta}{\sinh^2\xi + \sin^2\eta}\right\}. \tag{24}$$

		$\alpha = 10{\cdot}0$	$\alpha = 3{\cdot}33$	$\alpha = 1{\cdot}67$
(*a*) *Davidson model*				
Circular bubble	$k = 0; \tau = 1$	0·222	0·857	3·000
Indented bubbles	$k = 0{\cdot}286$	0·377	1·014	3·257
	$k = 0{\cdot}35$	0·482	1·129	3·461
	$k = 0{\cdot}40$	0·595	1·320	3·758
Elliptical bubbles	$\tau = 0{\cdot}875$	0·224	0·863	3·017
	$\tau = 0{\cdot}75$	0·231	0·885	3·078
	$\tau = 0{\cdot}625$	0·245	0·931	3·211
	$\tau = 0{\cdot}50$	0·273	1·022	3·469
(*b*) *Murray model*				
Circular bubble	$k = 0; \tau = 1$	0·110	0·422	1·476
Indented bubbles	$k = 0{\cdot}286$	0·277	0·636	1·849
	$k = 0{\cdot}35$	0·382	0·770	2·084
	$k = 0{\cdot}40$	0·505	0·928	2·358
Elliptical bubbles	$\tau = 0{\cdot}875$	0·104	0·398	1·390
	$\tau = 0{\cdot}75$	0·098	0·377	1·310
	$\tau = 0{\cdot}625$	0·094	0·359	1·239
	$\tau = 0{\cdot}50$	0·091	0·347	1·181

TABLE 2. Ratio (A_c/A_b) of cloud area to bubble area for circular and deformed bubbles

The cloud boundary is the closed branch of the $\psi_G = 0$ streamline†

$$(1-\alpha)e\sinh\xi + \frac{\alpha\tau(1+\tau)}{e(\cosh\xi+\sinh\xi)} + \frac{\tau^3}{2e^2} \times \frac{\cos\eta}{\sinh^2\xi + \sin^2\eta} = 0. \tag{25}$$

Cloud boundaries obtained from (25) are shown in figure 4 for $\tau = 0{\cdot}80$ and $\tau = 0{\cdot}60$ and for the values of α which have been employed in table 2 and figures 1 and 3. It is clear that the clouds predicted by Murray's model are roughly elliptical in shape but displaced forward somewhat, so that the centroid of the cloud area lies above the bubble centre as for undeformed bubbles. The clouds for

† It may be noted that the bubble boundary becomes circular as $\tau \to 1$. In this limit $e\sinh\xi \to r$, $e \to 0$, $\sinh\xi \to \cosh\xi \to \infty$, $\eta \to \theta$ and it can readily be shown that (22), (23) and (25) reduce to the corresponding expressions obtained by Davidson and Murray for undeformed bubbles.

elongated bubbles are smaller than for the corresponding circular bubble of the same area rising at the same dimensionless velocity α.

Cloud areas have been calculated by numerical integration and some values of A_c/A_b are given in table 2. Figure 5 shows how the cloud area changes as a bubble

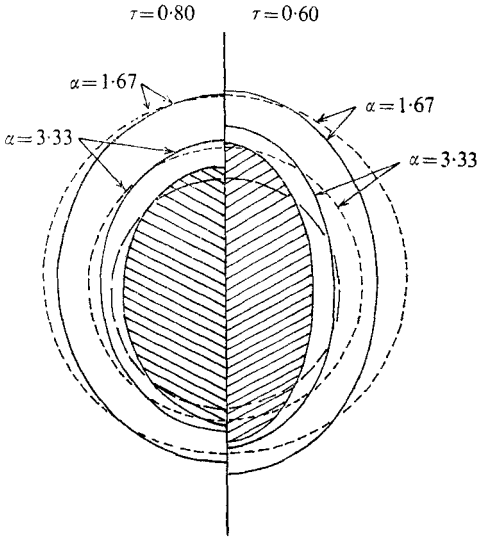

FIGURE 4. Cloud boundaries for elliptical bubbles: Murray theory. Notation as in figure 3.

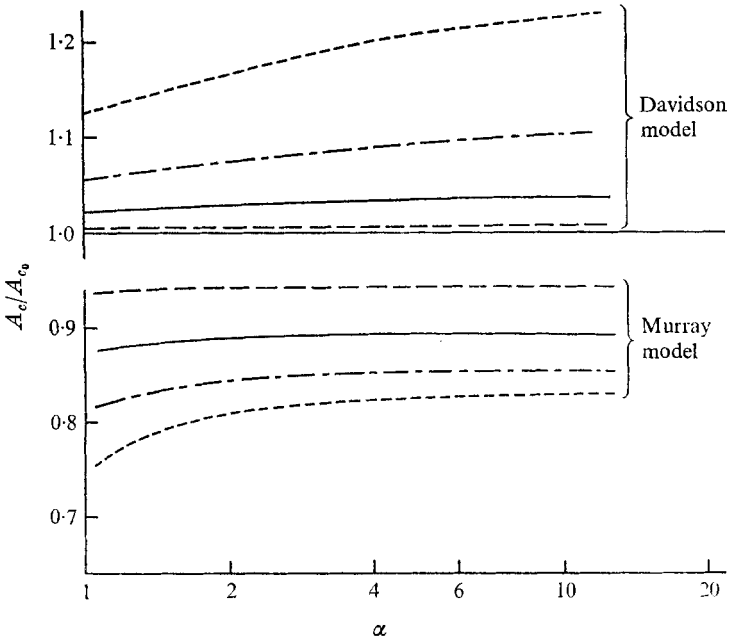

FIGURE 5. Ratio of cloud area for elliptical bubbles to cloud area for undeformed bubbles as a function of α. – – –, τ = 0·875; —, τ = 0·75; — · —, τ = 0·625; · · · · · ·, τ = 0·50.

becomes elongated while retaining the same value of α. It can be seen that the cloud is always larger than for the corresponding circular bubble for the Davidson model and smaller for Murray's model. Because the cloud area A_{c_0} for circular bubbles is already about twice as large for Davidson's model than for Murray's, bubble elongation tends to accentuate the discrepancy between the cloud areas and between the degree of gas–solid contact predicted by the two models.

4. Interacting bubbles in vertical alignment

In freely bubbling fluidized beds bubbles are constantly in the process of coalescing and splitting, so that interactions between bubbles are of great importance. In order to illustrate the effect of bubble interaction on gas–solid contacting we consider the flow around a pair of bubbles. For simplicity, wake effects and higher order bubble interactions are neglected.

Except under special circumstances the velocities of neighbouring bubbles are not identical, so that the flow is unsteady with respect to any set of axes and the basic equations for steady motion of gas and particles no longer apply. However, for a pair of bubbles of unequal size rising in a vertical line there is one particular spacing at which the relative velocity vanishes. The present analysis is limited to this particular case. The spacing between the bubbles is calculated from the interaction theory of Clift & Grace (1970, 1971*b*); a parallel but more complex theory due to Lin (1970) gives almost identical values (Clift & Grace 1971*a*). The procedure of choosing a particular situation in which bubbles interact but the motion is steady has also been employed by Gabor (1969) and Gabor & Koppel (1970) in analyses of gas and particle motion around an infinite vertical chain of equal-sized equally spaced bubbles.

The problem of solving Murray's equations for particle motion is to find a complex velocity potential which satisfies the boundary conditions of (i) uniform velocity $-U_B$ remote from the bubbles, (ii) no particle flow across the bubble boundaries. The representation of two exactly circular bubbles requires an infinite series of doublets for each bubble. Interacting bubbles are not completely circular; therefore the particle stream functions are kept to simple forms which satisfy the second boundary condition on closed surfaces which are approximately, but not exactly, circular. With Murray's model this also ensures that the gas stream function is relatively simple. On the other hand, the corresponding simple gas stream function for Davidson's model turns out to satisfy the constant pressure condition on a boundary which is slightly different from the boundary for the particle motion (Collins 1965; Gabor 1969). For this reason Davidson's method of analysis has not been pursued for interacting bubbles.

Each bubble is represented by a single doublet in the complex potential for the particle motion. If the doublets are situated at $(0, 0)$ and $(x_2, 0)$ in the z plane the particle complex potential relative to the bubbles is given by

$$w_P = -U_B\left\{z+\frac{a_1^2}{z}+\frac{a_2^2}{z-x_2}\right\}, \tag{26}$$

where a_1 and a_2 are the radii of the circular boundaries which each bubble would have in the absence of the other bubble.† It follows that the particle stream function is

$$\psi_P = -U_B y\left[1 - a_1^2\left\{\frac{1}{x^2+y^2} + \frac{s^2}{(x-x_2)^2+y^2}\right\}\right], \tag{27}$$

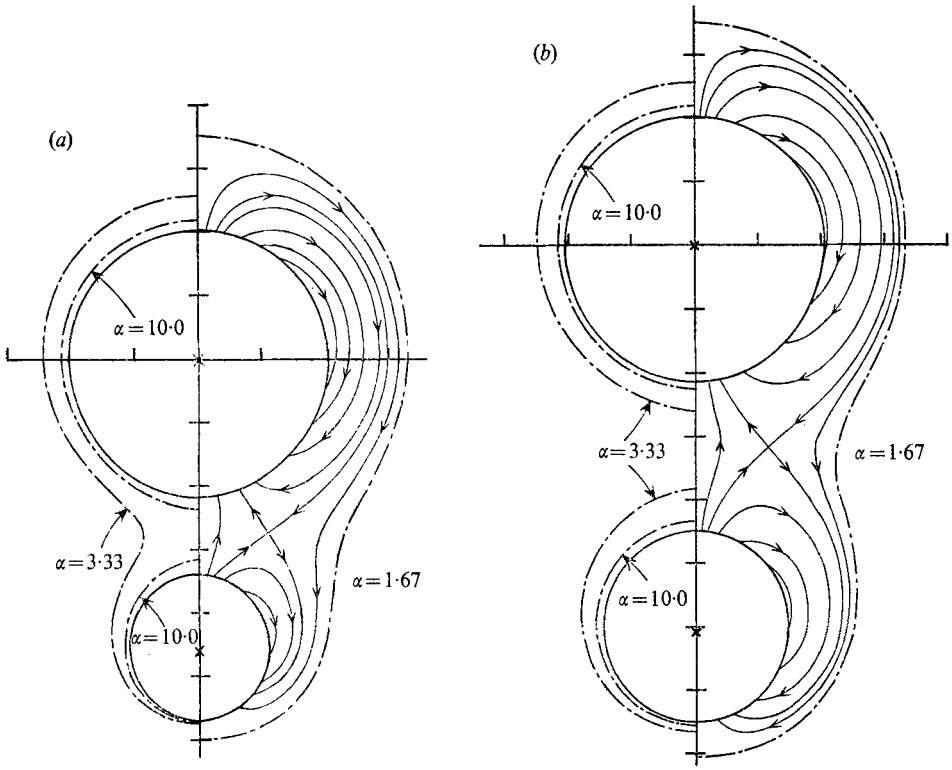

FIGURE 6. Cloud boundaries and gas streamlines for interacting bubbles in vertical alignment. (*a*) $s = 0{\cdot}5$, $x_2/a_1 = -2{\cdot}306$. (*b*) $s = 0{\cdot}7$, $x_2/a_1 = -3{\cdot}031$.

where $s = a_2/a_1$. The bubble boundaries are defined by the closed branch of the streamline $\psi_P = 0$; i.e.

$$a_1^2\left[\frac{1}{x^2+y^2} + \frac{s^2}{(x-x_2)^2+y^2}\right] = 1. \tag{28}$$

These boundaries are plotted in figure 6(*a*) for $s = 0{\cdot}5$, $x_2/a_1 = -2{\cdot}306$ and in figure 6(*b*) for $s = 0{\cdot}7$, $x_2/a_1 = -3{\cdot}031$, where the values of x_2 are chosen so that the bubbles have zero relative velocity. Figure 6 shows that the resulting bubble shapes are distorted in qualitatively the same manner as real interacting bubbles, although in practice rather more distortion is observed, especially for the rear bubble (Clift & Grace 1970).

† The bubble areas described by this model are somewhat greater than the areas described by doublets of the same strength remote from each other. For figure 6(*a*) the increase is 7 % for the leading bubble and 27 % for the rear bubble, while for figure 6(*b*) the increases are, respectively, 7 % and 14 %. Because bubbles in fluidized beds do tend to grow during the coalescence process, and because the model itself is only approximate, no correction to the doublet strengths has been made to offset this growth.

The complex potential for the gas motion around the interacting bubbles follows from (2) and (26):

$$w_G = u_0 z - U_B\left\{z + \frac{a_1^2}{z} + \frac{a_2^2}{z-x_2}\right\} - CFa_1\alpha\left\{\frac{a_1^2}{z^2} + \frac{a_2^2}{(z-x_2)^2}\right\}. \tag{29}$$

The value of the linearization constant C for interacting bubbles without relative velocity is expected to be only a few per cent different from the value for a

	$\alpha = 10$	$\alpha = 3{\cdot}333$	$\alpha = 1{\cdot}667$
Area ratio			
Leading bubble	0·129	—	—
Rear bubble	0·165	—	—
Overall	0·137	0·565	1·66
Values for isolated bubbles			
Uncorrected†	0·110	0·422	1·48
Leading bubble‡	0·115	0·451	1·62
Rear bubble‡	0·171	0·780	6·62
Overall‡	0·128	0·526	2·76

(*a*)

	$\alpha = 10$	$\alpha = 3{\cdot}333$	$\alpha = 1{\cdot}667$
Area ratio			
Leading bubble	0·131	0·496	—
Rear bubble	0·133	0·531	—
Overall	0·132	0·508	1·86
Values for isolated bubbles			
Uncorrected†	0·110	0·422	1·48
Leading bubble‡	0·116	0·455	1·65
Rear bubble‡	0·142	0·597	2·87
Overall‡	0·125	0·505	2·06

(*b*)

TABLE 3. Predicted cloud areas for interacting bubbles in vertical alignment. Values for ratio of cloud area to bubble area: (*a*) $s = 0{\cdot}5$, $x_2 = -2{\cdot}306$, (*b*) $s = 0{\cdot}7$, $x_2 = -3{\cdot}031$

† 'Uncorrected' values refer to isolated bubbles with the same α as interacting bubbles.
‡ These are 'corrected' values which refer to isolated bubbles with lower values of α, allowing for effect of interaction on bubble velocity.

corresponding isolated bubble (Clift & Grace 1971*a*), so that (10) may be used to eliminate CF from (29). The imaginary part of the resulting equation yields

$$\psi_G = u_0 y\left[1 - \alpha\left\{1 - a_1^2\left(\frac{1}{x^2+y^2} + \frac{s^2}{(x-x_2)^2+y^2}\right)\right\} + \frac{a_1^3}{2}\left\{\frac{x}{(x^2+y^2)^2} + \frac{s^2(x-x_2)}{[(x-x_2)^2+y^2]^2}\right\}\right]. \tag{30}$$

The cloud boundary is defined by the closed branch of the streamline $\psi_G = 0$, which follows from (30) as

$$\alpha\left[1 - a_1^2\left\{\frac{1}{x^2+y^2} + \frac{s^2}{(x-x_2)^2+y^2}\right\}\right] = 1 + \frac{a_1^3}{2}\left\{\frac{x}{(x^2+y^2)^2} + \frac{s^2(x-x_2)}{[(x-x_2)^2+y^2]^2}\right\}. \tag{31}$$

The resulting cloud boundaries are shown in figure 6 for three values of α. It is clear that even for $\alpha = 10$ the interaction between the two bubbles changes the cloud boundaries, causing each cloud to extend in the direction of the other. When α is sufficiently small the cloud boundaries combine so that a single cloud envelops both bubbles. Some gas streamlines within this joint cloud are also shown in figure 6 and are calculated from (30) for $\alpha = 1{\cdot}667$. An interchange of gas between the two bubbles from the lower to the upper bubble near the line of centres and in the reverse direction near the cloud boundary is predicted.†

The effect of interaction on cloud area is shown in table 3, where values are listed for the ratio of the cloud area to the bubble area. The values are 12 % to 34 % higher than the corresponding ratio for an isolated bubble with the same dimensionless velocity α. A more valid comparison is with isolated bubbles at lower α-values, since the effect of interaction is to increase the bubble velocity. This correction was applied using the theory of Clift & Grace (1970, 1971*b*), and the resulting values for the area ratio are also shown in table 3. For the larger values of α the predicted effect of interaction is still to increase the cloud area, the growth being at most 7·5 %. For $\alpha = 1{\cdot}667$ the predicted effect is a decrease in the cloud area of 40 % for $s = 0{\cdot}5$ and 10 % for $s = 0{\cdot}7$, this decrease being due to the rear bubble, which would have α close to unity and therefore a very large cloud, when in isolation.

5. Interacting bubbles in oblique alignment

Shichi, Mori & Muchi (1968) presented an analysis of gas and particle motion around two equal-sized bubbles which are not in vertical alignment, but which rise vertically without relative velocity. In actual fact, such bubbles would experience a small relative velocity (Clift & Grace 1971*b*). In this respect the treatment presented here is oversimplified but it is included in order to correct a misconception arising from the earlier work of Shichi *et al.*

Each bubble is represented by a single doublet in the particle equations as in the previous section. If the second doublet is located at $z_2 = x_2 + iy_2$ in the z plane and the bubbles are of equal size, then (26) and (27) are replaced by

$$w_P = -U_B\left[z + a_1^2\left(\frac{1}{z} + \frac{1}{z - z_2}\right)\right], \tag{32}$$

$$\psi_P = -U_B\left[y - a_1^2\left\{\frac{y}{x^2+y^2} + \frac{y - y_2}{(x-x_2)^2 + (y-y_2)^2}\right\}\right]. \tag{33}$$

Figure 7 shows the resulting particle streamlines for $y_2 = -x_2 = 2{\cdot}5$. This model does not describe closed bubble boundaries but Shichi *et al.* arbitrarily chose the circles centred on the doublets passing through the stagnation points as bubble boundaries. However, there is particle flow across these surfaces and this violates the second boundary condition for particle motion.

† This exchange from one bubble to another leads to an explanation of the leakage of gas between adjacent bubbles observed by Rowe, Partridge & Lyall (1964) and Rowe & Partridge (1965).

To obtain a better representation further terms must be added to (32) and (33). Higher image doublets might be added, but for equal-sized bubbles it is simpler to add terms representing a circulation Γ at the position of each doublet

$$w_P = -U_B\left[z + a_1^2\left(\frac{1}{z} + \frac{1}{z-z_2}\right) + i\Gamma\{\ln z - \ln(z-z_2)\}\right], \tag{34}$$

$$\psi_P = -U_B\left[y - a_1^2\left\{\frac{y}{x^2+y^2} + \frac{y-y_2}{(x-x_2)^2+(y-y_2)^2}\right\}\right.$$

$$\left. + \tfrac{1}{2}\Gamma\{\ln(x^2+y^2) - \ln[(x-x_2)^2+(y-y_2)^2]\}\right]. \tag{35}$$

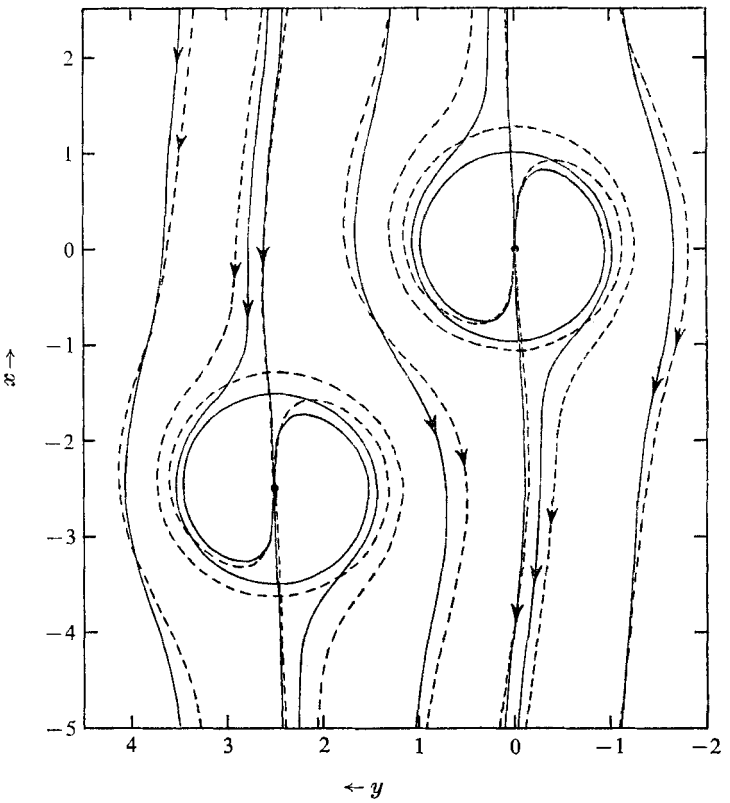

FIGURE 7. Particle and gas streamlines for bubbles in oblique alignment according to Shichi, Mori & Muchi (1968). Bubbles centred at (0, 0) and (−2·5, 2·5); $\Gamma = 0$; $\alpha = 3{\cdot}33$; ----, gas streamlines; —, particle streamlines.

Equations (34) and (35) still satisfy the boundary condition remote from the bubble, and if the value of Γ is chosen to bring the two particle stagnation points for each bubble onto the same particle streamline, the bubble boundary is closed and the second boundary condition is also satisfied. Figure 8 shows particle streamlines defined by (35) for $y_2 = -x_2 = 2{\cdot}5$ and $\Gamma = -0{\cdot}41251$. The resulting bubble boundaries are seen to be closed and almost circular.

The complex potential for the gas motion is obtained from (2) and (34), where CF is again approximated by its value for an isolated bubble. On taking the imaginary part of the resulting expression, we may write

$$\psi_G = y + \alpha\psi_P + \frac{1}{2}\left\{\frac{xy}{(x^2+y^2)^2} + \frac{(x-x_2)(y-y_2)}{[(x-x_2)^2+(y-y_2)^2]^2}\right\} + \frac{\Gamma}{4}\left\{\frac{x}{x^2+y^2} - \frac{x-x_2}{(x-x_2)^2+(y-y_2)^2}\right\}. \quad (36)$$

The stream function used by Shichi, Mori & Muchi does not include the circulation term, and the resulting gas streamlines are plotted in figure 7 for $y_2 = -x_2 = 2{\cdot}5$ and $\alpha = 3{\cdot}333$. There is no cloud boundary in the usual sense and the streamlines show flow of gas through the bubbles. For smaller separations, gas flows through both bubbles in series.

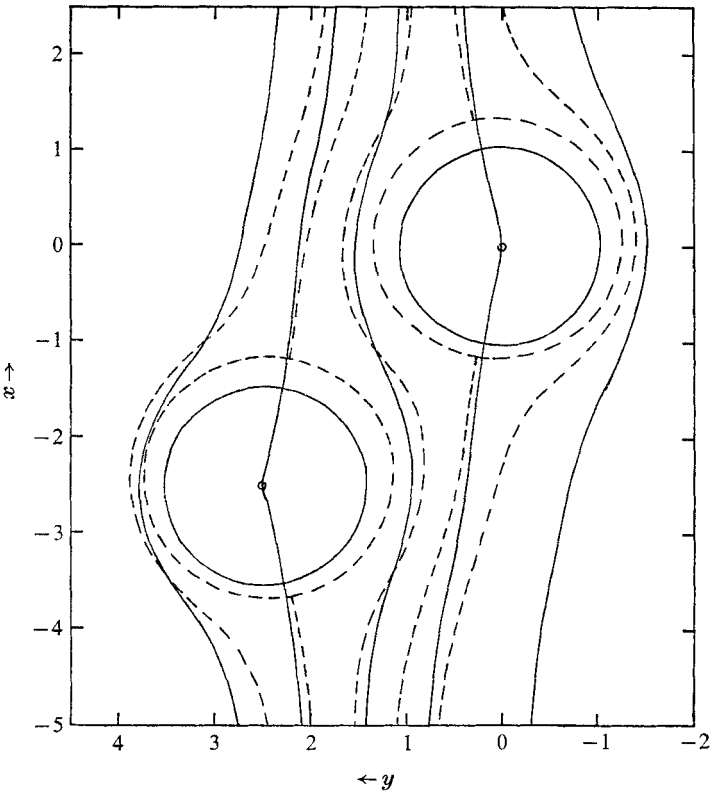

FIGURE 8. Particle and gas streamlines for bubbles in oblique alignment. Bubbles centred at (0, 0) and (−2·5, 2·5); $\Gamma = -0{\cdot}41251$; $\alpha = 3{\cdot}33$; – – –, gas streamlines; —, particle streamlines.

Figure 8 shows gas streamlines plotted with Γ chosen to close the particle streamlines. It is clear that closing the bubble boundaries also closes the gas streamlines, and normal cloud boundaries result. Thus the degeneracy of bubble clouds predicted by Shichi *et al.* (1968) results from failure to have closed particle streamlines; our analysis shows that clouds do exist for steady flows even when bubbles interact.

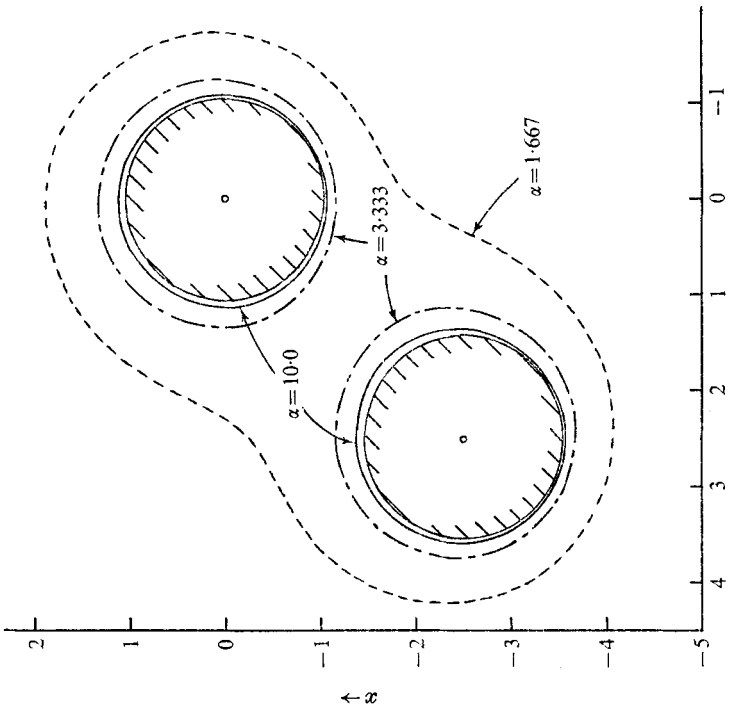

FIGURE 9. Cloud boundaries for interacting bubbles in oblique alignment. Bubbles centred at (0, 0) and (−3, 3); $\Gamma = -0{\cdot}34024$.

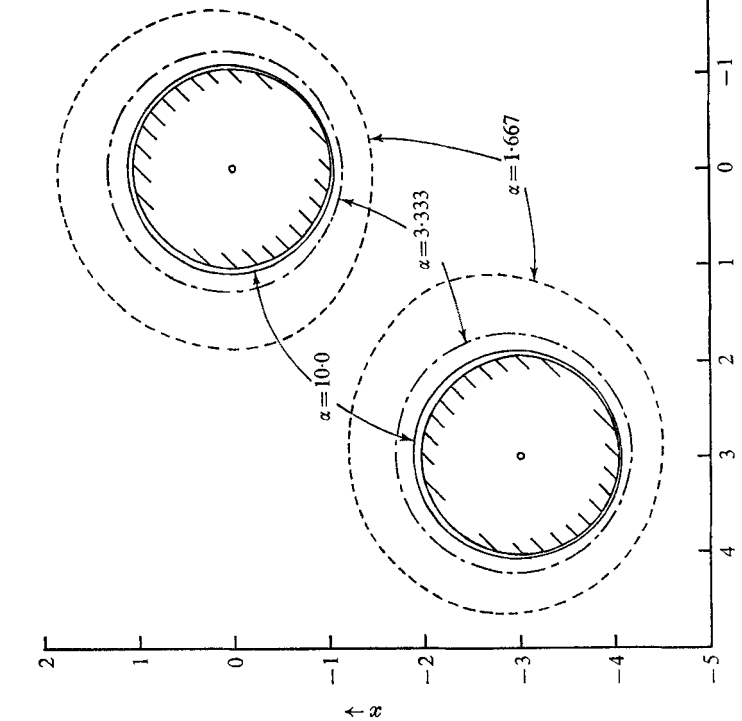

FIGURE 10. Cloud boundaries for interacting bubbles in oblique alignment. Bubbles centred at (0, 0) and (−2·5, 2·5); $\Gamma = -0{\cdot}41251$.

The cloud boundaries for two bubble separations and for three values of α are plotted in figures 9 and 10. For $\alpha = 1{\cdot}667$ the gas streamlines did not quite close for either case. However, the flow of gas through the region shown as the cloud was in each case less than 1 % of the gas flow across a horizontal section of width x_2 remote from the bubbles. Such a small flow almost certainly results from approximations in the solution and closed cloud boundaries have therefore been drawn. The clouds only distort significantly from the shapes associated with isolated bubbles at $\alpha = 1{\cdot}667$, the lowest value of α employed. Two bubbles are enclosed by a single cloud for $y_2 = -x_2 = 2{\cdot}5$ as shown in figure 10 and gas then flows between the bubbles as in figure 6.

6. Concluding remarks

The study of interacting bubbles presented in the last two sections has been limited to cases where there is no relative motion between two bubbles; when relative motion exists, the analysis becomes more complex. Toei, Matsuno, Nishitani, Hayashi & Imamoto (1969) applied Murray's equations to a pair of coalescing bubbles and predicted cloud boundaries which differ considerably from those presented in this paper and in the analyses of Gabor (1969), Gabor & Koppel (1970) and Shichi *et al.* (1968). However, the analysis of Toei *et al.* uses equations of steady gas and particle motion to describe an unsteady flow and, moreover, the meaning of clouds for unsteady situations must be considered carefully. For steady flows, streamlines and pathlines are identical so that a cloud boundary defines the limiting pathline for gas elements which spend some of their time in bubbles. For unsteady flows, it is possible to locate instantaneous closed gas streamlines when the bubble velocity exceeds u_0 but these streamlines do not define gas pathlines and therefore should not be regarded as cloud boundaries.

Experimental measurements obtained by Toei *et al.* in the same study indicate that a large increase in gas–solid contacting accompanies bubble coalescence in fluidized beds. Part of this increase is accounted for by the interaction effects discussed in the previous sections but a full account of this phenomenon awaits an analysis based on the equations of unsteady motion.

REFERENCES

Clift, R. & Grace, J. R. 1970 *Chem. Engng Progr. Symp.* Ser. **66**, no. 105, 14.

Clift, R. & Grace, J. R. 1971*a* *A.I.Ch.E. J.* **17**, 252.

Clift, R. & Grace, J. R. 1971*b* *Chem. Engng. Progr. Symp. Ser.* **67**, to appear.

Collins, R. 1965 *Chem. Engng Sci.* **20**, 747.

Davidson, J. F. 1961 *Trans. Instn Chem. Engrs.* **39**, 230.

Davidson, J. F. & Harrison, D. 1963 *Fluidised Particles.* Cambridge University Press.

Gabor, J. D. 1969 *Ind. Engng Chem. Fund,* **8**, 84.

Gabor, J. D. & Koppel, L. B. 1970 *Chem. Engng Progr. Symp. Ser.* **66** (105), 28.

Grace, J. R. 1970 *Can. J. Chem. Engng.* **48**, 30.

Grace, J. R. & Harrison, D. 1967 *Chem. Engng Sci.* **22**, 1337.

Grace, J. R. & Harrison, D. 1968 *Symposium on the Engineering of Gas–Solid Reactions,* p. 93. London: Instn. Chem. Engrs.

GRACE, J. R. & HARRISON, D. 1969 *Chem. Engng Sci.* **24**, 497.

JACKSON, R. 1963*a* *Trans. Instn Chem. Engrs.* **41**, 13.

JACKSON, R. 1963*b* *Trans. Instn Chem. Engrs.* **41**, 22.

KUNII, D. & LEVENSPIEL, O. 1969 *Fluidization Engineering.* Wiley.

LIN, S. P. 1970 *A.I.Ch.E. J.* **16**, 130.

LOCKETT, M. J. & HARRISON, D. 1967 *Proc. Int. Fluidisation Symp.* p. 257. Amsterdam: Netherlands University Press.

MILNE-THOMSON, L. M. 1962 *Theoretical Hydrodynamics,* 4th ed. Macmillan.

MURRAY, J. D. 1965*a* *J. Fluid Mech.* **21**, 465.

MURRAY, J. D. 1965*b* *J. Fluid Mech.* **22**, 57.

PARLANGE, J. Y. 1969 *J. Fluid Mech.* **37**, 257.

PYLE, D. L. & ROSE, P. L. 1965 *Chem. Engng Sci.* **20**, 25.

REUTER, H. 1963 *Chem. Ing. Tech.* **35**, 98.

ROWE, P. N. 1964 *Chem. Engng Progr.* **60** (3), 75.

ROWE, P. N. & PARTRIDGE, B. A. 1962 *Symposium on Interactions between Fluids and Particles,* p. 135. London: Instn. Chem. Engrs.

ROWE, P. N. & PARTRIDGE, B. A. 1965 *Trans. Instn Chem. Engrs.* **43**, 157.

ROWE, P. N., PARTRIDGE, B. A., CHENEY, A. G., HENWOOD, G. A. & LYALL, E. 1965 *Trans. Instn Chem. Engrs.* **43**, 271.

ROWE, P. N., PARTRIDGE, B. A. & LYALL, E. 1964 *Chem. Engng. Sci.* **19**, 973.

SHICHI, R., MORI, S. & MUCHI, I. 1968 *Kagaku Kogaku,* **32**, 343.

STEWART, P. S. B. 1968 *Trans. Instn Chem. Engrs.* **46**, 60.

TOEI, R., MATSUNO, R., NISHITANI, K., HAYASHI, H. & IMAMOTO, T. 1969 *Kagaku Kogaku,* **33**, 668.